Heliyon

Received:
28 July 2017
Revised:
12 December 2017
Accepted:
28 January 2018

Cite as: Francesco Fornarelli, Ruggiero Dadduzio, Marco Torresi, Sergio Mario Camporeale, Bernardo Fortunato. Three-dimensional analysis of flow-chemical interaction within a single square channel of a lean NO_x trap catalyst. Heliyon 4 (2018) e00529. doi: 10.1016/j.heliyon.2018.e00529

Three-dimensional analysis of flow-chemical interaction within a single square channel of a lean NO_x trap catalyst

Francesco Fornarelli *, **Ruggiero Dadduzio, Marco Torresi, Sergio Mario Camporeale, Bernardo Fortunato**

Polytechnic University of Bari, Department of Mechanics, Mathematics and Management, via Orabona, 4, 70125 Bari, Italy

* Corresponding author.
E-mail address: francesco.fornarelli@poliba.it (F. Fornarelli).

Abstract

A fully 3D unsteady Computational Fluid Dynamics (CFD) approach coupled with heterogeneous reaction chemistry is presented in order to study the behavior of a single square channel as part of a Lean NO_x Traps. The reliability of the numerical tool has been validated against literature data considering only active BaO site. Even though the input/output performance of such catalyst has been well known, here the spatial distribution within a single channel is investigated in details. The square channel geometry influences the flow field and the catalyst performance being the flow velocity distribution on the cross section non homogeneous. The mutual interaction between the flow and the active catalyst walls influences the spatial distribution of the volumetric species. Low velocity regions near the square corners and transversal secondary flows are shown in several cross-sections along the streamwise direction at different instants. The results shed light on the three-dimensional characteristic of both the flow field and species distribution within a single square channel of the catalyst with respect to 0-1D approaches.

Keywords: Mechanical engineering, Computational mathematics

https://doi.org/10.1016/j.heliyon.2018.e00529

1. Introduction

Lean-burn diesel engines have been encouraged due to both their high fuel efficiency and the reduction of HC and CO_2 emissions. However, the lean-burn combustion generates NO_x, a pollutant responsible of harmful consequences on environment and human health. In order to meet Post-Euro6 regulations on emissions of diesel engines for vehicle homologation, the layout of the Exhaust Gas Treatment (EGT) system is requested to meet the emission limits under highly variable driving cycles such as the Worldwide harmonized Light Test Cycle (WLTC). Furthermore, the legislation requires the direct measurements on board, installing a Portable Emission Measurement System (PEM) on the vehicle. Hence, the reduction of NO_x emissions represents one of the most challenging problem on which engineers and scientists are working on. The Lean NO_x Trap (LNT), also known as NO_x Storage Catalyst (NSC), is the most practical abatement approach with respect to the Selective Catalytic Reduction (SCR) device, e.g. avoiding the implementation of urea injection devices. On the other hand, the LNT catalyst needs a more complex controlling strategy, switching between rich and lean conditions in the combustion process. Thus, the prediction of the catalyst behavior with respect to the controlled parameters, such as the inlet velocity, the species concentrations, temperature, etc., still represents a challenge. The review work of Roy and Baiker (2009) gives a comprehensive overview on the state of the art of LNT. In order to describe the chemical reactions in a LNT catalyst, several approaches can be found in the literature, among them: either detailed or microkinetic mechanisms and global kinetic models. Usually, due to the great number of reactions involved in the mechanism, detailed and microkinetic models are implemented in 0-1D codes (i.e. constantly stirred tank reactors, CSTR and plug flow reactors, PFR), where the kinetic parameters are tuned according to experimental measurements (Bhatia et al., 2009; Cao et al., 2008; Kota et al., 2015; Larson et al., 2012; Lindholm et al., 2008; Shwan et al., 2014; Xu et al., 2008, 2009). In particular, Olsson et al. (2001) developed a detailed NO_x storage-oxidation mechanism over Pt/BaO that has been extensively used and improved (Rankovic et al., 2010; Scotti et al., 2004). Olsson et al. (2001) implemented mean field model, describing the monolith as a series of 15 continuously stirred tank reactors, achieving fair results with respect to the measurements. The reliability of the model is confirmed by other works (Rankovic et al., 2010; Scotti et al., 2004), where further improvements of the same chemical mechanism can be found. A one dimensional code coupled to the chemical solution of detailed microkinetic mechanism was presented by Larson et al. (2012) and Kota et al. (2015): in both of these mechanisms the diffusion through the washcoat was considered. A two-dimensional model of the flow field in a single channel was developed by Koop and Deutschmann (2007) where a shrinking core model (Olsson et al., 2005) has been used and in Koop and Deutschmann (2009)

 https://doi.org/10.1016/j.heliyon.2018.e00529

with a detailed surface reaction mechanism. Usually, only the slowest reactions involved in the NO_x adsorption were considered. For instance, Benjamin and Roberts (2007) implement a simplified flow through a porous medium with a simplified heterogeneous mechanism (Laurent et al., 2003). Kočí et al. (2006) evaluated the physical and chemical behavior of porous catalysts. Their work is focused on the washcoat structure influence at microscale. Porous matrix is considered considering simplified transport diffusion equation for the species. The approach is interesting for porous medium, however this model cannot give details of the flow field and species distribution within a channel flow with surface reaction. Chen et al. (2004) consider a porous medium approach in which the detail of the spatial distribution of flow and species within a single channel is missing. On the other hand, Corbetta et al. (2014) make comparison between the numerical and experimental results in case of diluted reacting flow. Their approach decouples the flow field and the chemical reactions. First, a steady solution of the non-reactive flow field is achieved and then, in post-processing, the transport diffusion equation for each species is solved considering the chemical reactions completely decoupled with respect to the flow field. A fully coupled three-dimensional reactive flow model has been proposed by Maestri and Cuoci (2013). They propose a mathematical model to fully couple flow and reactive flow implementing a post-processing of the non-reacting flow. They analyze a particular reactor highlighting how the hydrodynamic affects the results. They confirm that in highly diluted reactive heterogeneous system the fluid dynamic of the reacting flow cannot be neglected. Štěpánek et al. (2012) considered three dimensional non reactive flow solved by CFD coupled with a 1D channel model for the solution of the reacting channel flow of the active matrix. In fact, the active matrix is supposed to be made of multi-channel geometry. Therefor, the three-dimensional spatial distribution within a single channel is missing. Three-dimensional fully coupled unsteady reacting flow study of NSC catalysis is still limited to few preliminary works (Fornarelli et al., 2015; Mihet et al., 2016).

Here, a fully coupled three-dimensional unsteady reactive flow simulation is presented. A well-known experimental test (Olsson et al., 2001) has been reproduced implementing a detailed reaction mechanism of NO_x adsorption over BaO. Indeed, during the lean phase, the alkali earth storage component (BaO) stores the NO_x generating nitrites and nitrates. A validation study is reported comparing the overall output of the present study and the experimental and numerical findings of Olsson et al. (2001). Particular care has been used in the treatment and analysis of the influence of the channel geometry (square channel) on the catalyst performance. Thus, the three-dimensional flow field and species distribution are shown, describing their mutual influence in a single square catalyst channel.

 https://doi.org/10.1016/j.heliyon.2018.e00529

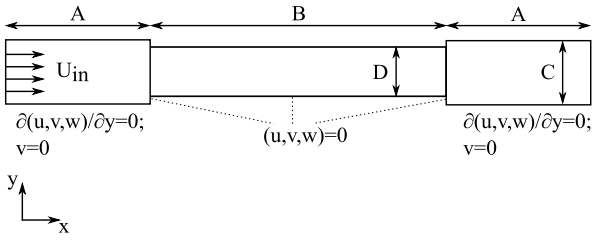

Figure 1. Schematic of the numerical domain and the boundary conditions. u, v, w represent the velocity components with respect x, y, z directions.

Table 1. Table of catalyst dimensions.

Description	ref. in Figure 1	[mm]
Channel length	B	15
Inlet/Outlet zone length	A	10
Channel side	D	0.9
Inlet/outlet side	C	1.2

2. Model

The validation process of the NO_x Storage chemical model coupled with the CFD solution has been performed by means of a Direct Numerical Simulation (DNS) of the Navier–Stokes equations. The computational domain consists in a single square channel of the monolith used in the work of Olsson et al. (2001). In order to better reproduce the flow at the inlet and outlet section of the square channel, two zones at inlet and outlet, both marked as A in Figure 1, are considered where the inlet and outlet boundary conditions on the velocity and the pressure are imposed, respectively. On the side surfaces of both the zones A, symmetry boundary conditions are imposed. Instead, no-slip boundary conditions are imposed on the walls of the square channel of the catalyst (zone B). In Table 1, the main geometrical characteristic of the computational domain are reported with reference to Figure 1. In all the tests here considered a flow rate of 37.7 ml/min has been taken into account.

The reactive flow field in the catalyst was simulated by means of the ANSYS Fluent flow solver. The Reynolds Number of the experiment, based on the mean velocity and the hydraulic diameter of the channel, is about 13. Due to the detailed heterogeneous chemical mechanism, the reactions do not take place in the gaseous phase, but only on the solid surfaces of the channel. The density and viscosity variations due to the mixture composition and the flow temperature are also taken into account in the simulation. The governing equations read as follows:

$$\frac{\partial \rho}{\partial t} + \nabla \cdot (\rho \vec{v}) = 0$$

$$\frac{\partial}{\partial t}(\rho \vec{v}) + \nabla \cdot (\rho \vec{v} \vec{v}) = -\nabla p + \nabla \cdot \overline{\overline{\tau}} + \overline{F}$$

$$\frac{\partial}{\partial t}(\rho E) + \nabla \cdot (\vec{v}(\rho E + p)) = \nabla \cdot (k_{eff} \nabla T - \sum_j h_j \vec{J}_j + (\overline{\overline{\tau}}_{eff} \cdot \vec{v})) + S_h$$

https://doi.org/10.1016/j.heliyon.2018.e00529

for mass, momentum and energy conservation, respectively, where ρ is the mixture density, $\vec{v}$ the velocity vector, p the pressure, $\overline{\overline{\tau}}$ the viscous stress tensor, $\overline{F}$ the momentum source term, E the total energy of the system, k_{eff} the effective conductivity, $\vec{J}_j$ the diffusion flux of species j and S_h the energy sources, which includes the heat of chemical reactions. The diffusion flux of species j, due to the gradients of concentration and temperature, $\overrightarrow{J_j}$, is defined by:

$$\overrightarrow{J_j} = -\rho\gamma_{j,m}\nabla Y_j - \gamma_{T,i}\frac{\nabla T}{T}$$

where $\gamma_{i,m}$ is the mass diffusion coefficient and $\gamma_{T,i}$ is the thermal diffusion coefficient for species i. For the gas mixture, the transport equation of each species mass fraction Y_k has been considered in the form:

$$\frac{\partial \rho Y_k}{\partial t} + \frac{\partial}{\partial x_i}\left(\rho v_i Y_k - \gamma_k \frac{\partial Y_k}{\partial x_i}\right) = S_{Y_k} \tag{1}$$

γ_k is the diffusion coefficient and S_k the source term for the species k.

In order to solve the chemical reactions between different species at the surface, a heterogeneous chemical kinetic model has been considered. The model is applied in each cell bounded by the channel solid walls, where the concentration of different species may vary also due to the advection diffusion equation of the species (see equation (1)). The internal diffusion of the species within the washcoat can be neglected according to the large pore dimension (about 50 nm) of the test (Wickman et al., 2007). For the generic r_{th} reversible surface reaction, the reaction rate is

$$\mathcal{R}_r = k_{f,r}\prod_i^{N_g}[G_i]_{wall}^{g'_{i,r}}\prod_i^{N_s}[S_j]_{wall}^{s'_{j,r}} - k_{b,r}\prod_i^{N_g}[G_i]_{wall}^{g''_{i,r}}\prod_i^{N_s}[S_j]_{wall}^{s''_{j,r}}$$

where $[G_i]_{wall}$ is the volumetric concentration of the i_{th} gas species facing the solid wall and $[S_i]_{wall}$ is the surface concentration of the i_{th} species on the wall. $k_{f,r}$ and $k_{b,r}$ represent the forward and the backward rate constants for reaction r_{th}, respectively. The site coverage dependence is taken into account by according to Arrhenius expression:

$$k_{f,r} = A_r T^{\beta_r} e^{\frac{-E_{a,r}}{RT}} \prod_i (10^{Z_i\eta_{i,r}})(Z_i^{\mu_{i,r}})(e^{\frac{-\epsilon_{i,r}Z_i}{RT}}) \tag{2}$$

where A_r is the pre-exponential factor, $E_{a,r}$ is the activation energy, β_r the temperature exponent, $\epsilon_{i,r}$ is the activation energy dependent by the surface coverage of the i_{th} species, Z_i, defined as

$$Z_i = \frac{[S_i]}{\Gamma}$$

in which Γ represents the surface site density. On the solid surfaces, the mass flux of each species normal to the wall is imposed to be equal to its rate of production,

$$\rho_{wall}\gamma_i\frac{\partial Y_{i,wall}}{\partial n} = M_{w,i}\hat{R}_{i,gas}$$
$$\Gamma\frac{\partial Z_i}{\partial t} = \hat{R}_{i,site}$$

Table 2. Storage process reaction scheme.

#Reaction			Reversible Reactions
R1	$NO_{2(g)}$+BaO	⇌	BaO–NO_2
R2	BaO–NO_2	⇌	BaO–O+$NO_{(g)}$
R3	$NO_{2(g)}$+BaO–O	⇌	BaO–NO_3
R4	$NO_{2(g)}$+BaO–NO_3	⇌	$Ba(NO_3)_2$
R5	2BaO–O	⇌	2BaO+$O_{2(g)}$

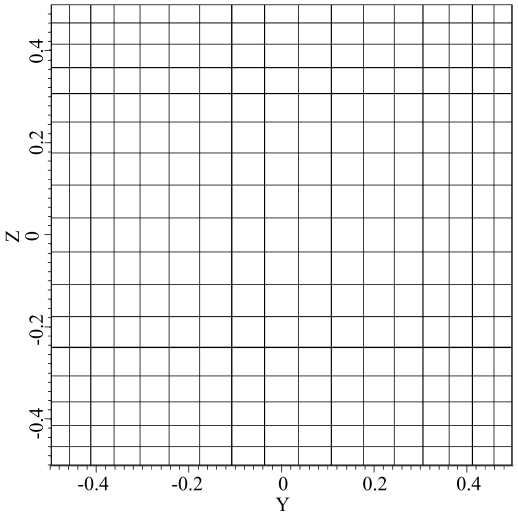

Figure 2. Detail of the grid resolution (grid 1) in the transversal section of the catalyst square channel at $x = 7.5$.

where $\hat{R}_{i,gas}$ and $\hat{R}_{i,site}$ are the net molar rates of either production or consumption, respectively, for gas and surface phases of the species, defined as:

$$\hat{R}_{i,gas} = \sum_{r}^{N_{reaction}} (g''_{i,r} - g'_{i,r})\mathcal{R}_r$$

$$\hat{R}_{i,site} = \sum_{r}^{N_{reaction}} (s''_{i,r} - s'_{i,r})\mathcal{R}_r$$

In order to perform a grid sensitivity of the numerical model, two meshes were considered. Moreover, in order to check the influence of the timestep on the solution two timesteps have been used.

The test consists in the inlet of 680 ppm of NO_2 at 350 °C for 600 s, according to the results presented in Olsson et al. (2001). The NO_x storage kinetic model on BaO used for the test is reported in Table 2. The overall numbers of cell of the two grids are 27528 for the coarser (Grid 1) and 106824 for the finer (Grid 2). The timesteps used are 0.1 s and 0.05 s for grid 1 and grid 2, respectively. The grids considered are structured and non-uniform in order to reduce the cell dimension near the solid walls (see Figure 2). The stretching of the mesh for the coarser and the finer grid are

 https://doi.org/10.1016/j.heliyon.2018.e00529

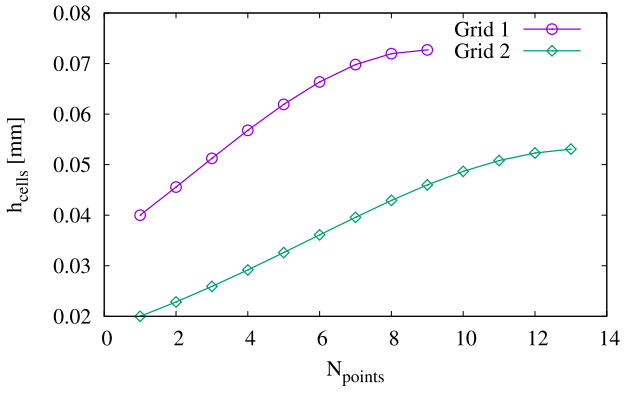

Figure 3. Cell heights with respect to the cell number along the side of the square channel are reported for coarser (grid 1) and finer (grid 2) grids.

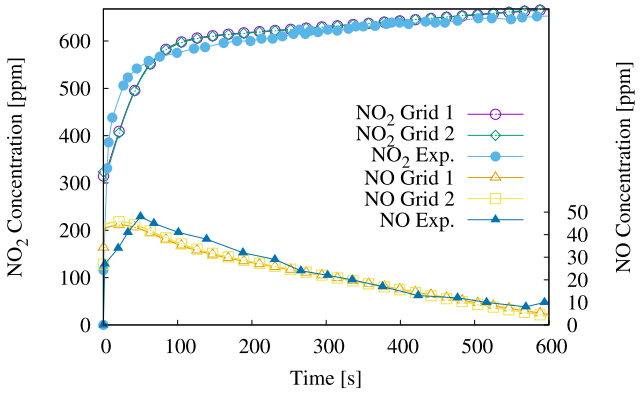

Figure 4. Comparison of NO_2 and NO concentrations with respect to the experiment of the BaO catalyst of Olsson et al. (2001). Grid 1: coarse grid with $dt = 0.1$ s, Grid 2: fine grid with $dt = 0.05$ s.

reported in Figure 3, where the cell heights with respect to the cell number along the side of the square channel are reported.

In Figure 4 the time history of the volumetric concentrations of both NO_2 and NO at the channel outlet are reported. The reported data confirm a satisfactory grid independence of the results and a good agreement with the experimental measurements. Thus, in order to optimize the computational cost, grid 1 and a timestep of 0.1 s has been used in all the numerical tests here presented. Moreover the spatial distributions of NO_2 concentrations along the axis at two different instants for grid 1 and grid 2 are reported in Figure 5.

3. Results and discussion

Active sites of a single type catalyst is considered on the washcoat. Actually, the model consists in sites of BaO over an Al_2O_3 support, where the NO_2 can be stored. The kinetic reaction mechanism used for the storage process includes five different

https://doi.org/10.1016/j.heliyon.2018.e00529

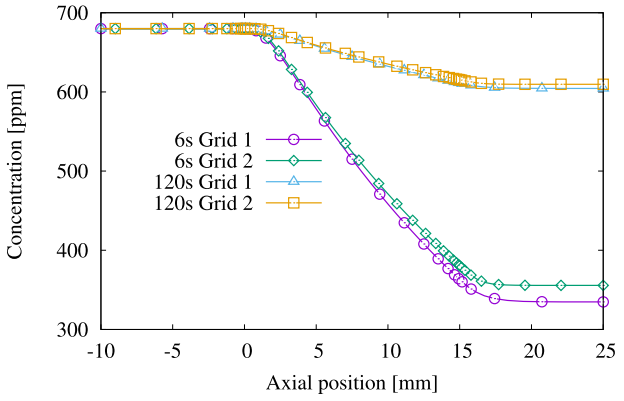

Figure 5. Comparison of NO_2 concentrations with respect to the axis of the channel at $t = 6$ s and $t = 120$ s for Grid 1 (coarse) and Grid 2 (fine). The NO_x storage kinetic model on BaO used for the test is reported in Table 2.

Table 3. Kinetic parameters of BaO site catalyst.

Reaction rate	Pre-exponential Factor	Activation Energy $[\frac{J}{kmol}]$
$R1_f = k_{1,f} C_{NO_{2(g)}} \theta_{BaO}$	$A_{1,f} = 707951\ [\frac{m^3}{s\ kmol}]$	$E_{1,f} = 27.9 \cdot 10^6$
$R1_b = k_{1,b} \theta_{BaO-NO_2}$	$A_{1,b} = 1 \cdot 10^{13}\ [\frac{1}{s}]$	$E_{1,b} = 186.4 \cdot 10^6$
$R2_f = k_{2,f} \theta_{BaO-NO_2}$	$A_{2,f} = 1 \cdot 10^{13}\ [\frac{1}{s}]$	$E_{2,f} = 151.8 \cdot 10^6$
$R2_b = k_{2,b} C_{NO_{(g)}} \theta_{BaO-O}$	$A_{2,b} = 6 \cdot 10^7\ [\frac{m^3}{s\ kmol}]$	$E_{2,b} = 0$
$R3_f = k_{3,f} C_{NO_{2(g)}} \theta_{BaO-O}$	$A_{3,f} = 3.36 \cdot 10^7\ [\frac{m^3}{s\ kmol}]$	$E_{3,f} = 0$
$R3_b = k_{3,b} \theta_{BaO-NO_3}$	$A_{3,b} = 1 \cdot 10^{13}\ [\frac{1}{s}]$	$E_{3,b} = 130.4 \cdot 10^6$
$R4_f = k_{4,f} C_{NO_{2(g)}} \theta_{BaO-NO_3}$	$A_{4,f} = 62742\ [\frac{m^3}{s\ kmol}]$	$E_{4,f} = 19.1 \cdot 10^6$
$R4_b = k_{4,b} \theta_{Ba(NO_3)_2}$	$A_{4,b} = 1 \cdot 10^{13}\ [\frac{1}{s}]$	$E_{4,b} = 250.5 \cdot 10^6$
$R5_f = k_{5,f} \theta^2_{BaO-O}$	$A_{5,f} = 1.83 \cdot 10^{18}\ [\frac{m^2}{s\ kmol}]$	$E_{5,f} = 196.9 \cdot 10^6$
$R5_b = k_{5,b} C_{O_{2(g)}} \theta^2_{BaO}$	$A_{5,b} = 1.38 \cdot 10^8\ [\frac{m^5}{s\ kmol^2}]$	$E_{5,b} = 68.6 \cdot 10^6$

reversible reactions (see Table 2), where the kinetic parameters, with a BaO site density equal to $\Gamma_{BaO} = 5.47343 \cdot 10^{-6}\ \frac{kmol}{m^2}$, are listed in Table 3. The mechanism is similar to the Olsson et al. (2001), centering the values with uncertainty.

In reference to reaction $R_{4,b}$, a variable activation energy with respect to the site coverage of the barium nitrate, that reads $\varepsilon_{4,b}(\vartheta_{Ba(NO_3)_2}) = -45.09 \cdot 10^6\ [\frac{J}{kmol}]$, is imposed with reference to the equation (2).

In Figure 6 the comparison of the volumetric concentrations of NO_2 and NO against the experimental and numerical findings of Olsson et al. (2001) are reported. The test consists in the following steps on a BaO catalyst: inlet mass flow rate with 680 ppm of NO_2 at 350 °C for 600 s, 60 s of pure N_2, 600 ppm of NO for 240 s and, at the end, a temperature increase up to 600 °C. The present model shows a good agreement with the reference case both in the first NO_2 phase and in the following NO phase. In the NO phase, the temperature ramp of 20 °C/min from 350 °C to

https://doi.org/10.1016/j.heliyon.2018.e00529

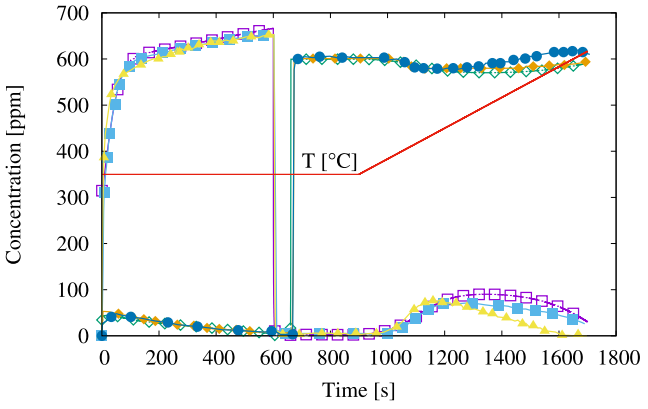

Figure 6. Comparison of the surface averaged concentrations, at the outlet of the channel, against the experimental and numerical findings of Olsson et al. (2001). NO_2: present (□), numerical (Olsson et al., 2001) (■), experimental (Olsson et al., 2001) (▲), NO: present (◇), numerical (Olsson et al., 2001) (◆), experimental (Olsson et al., 2001) (●).

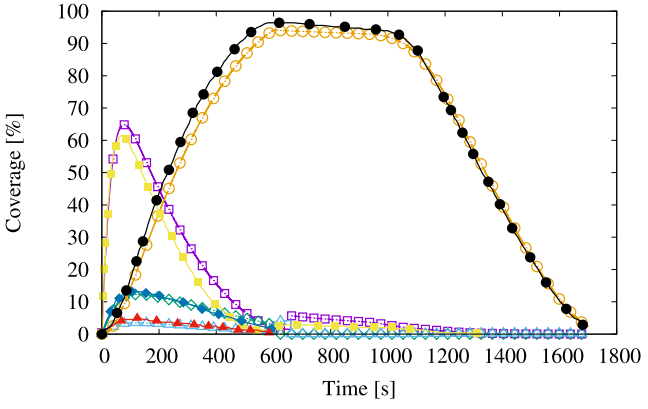

Figure 7. Comparison between the coverages, averaged over the channel side walls, evaluated by the CFD simulation and the theoretical curves presented in Olsson et al. (2001). Current results are marked with open symbols, Olsson et al. (2001) filled symbols. BaO–NO_2 (□, ■), BaO–NO_3 (◇, ◆), BaO–O (△, ▲), $Ba(NO_3)_2$ (○, ●).

600 °C leads to a small underestimation (overestimation) of NO (NO_2) with respect to the experimental measurements. However, the present results remark the behavior of the numerical model of Olsson et al. (2001). The surface coverages of the species at the wall have been reported in Figure 7 and compared with those calculated with the simplified model of Olsson et al. (2001). Thus, the predicted coverages are in fair agreement with the literature data without any relevant modification of the kinetic parameters described in Olsson et al. (2001). The O_2 concentrations, reported in Figure 8, have a maximum at $t = 114$ s. It represents the time response of the flow-chemical model during the first 600 s of test. The O_2 concentrations are very small according to the related reactions rate, $R5$, dependence to the square of the BaO coverage, $\propto \theta^2_{BaO}$, as reported in Table 3.

https://doi.org/10.1016/j.heliyon.2018.e00529

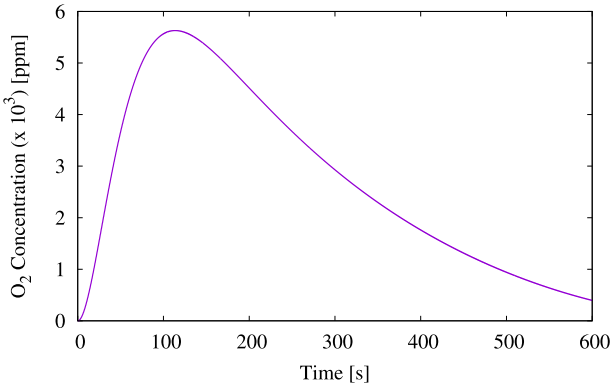

Figure 8. Surface averaged O_2 concentration at the channel outlet with respect to the time during the NO_2 phase (t = 0–600 s).

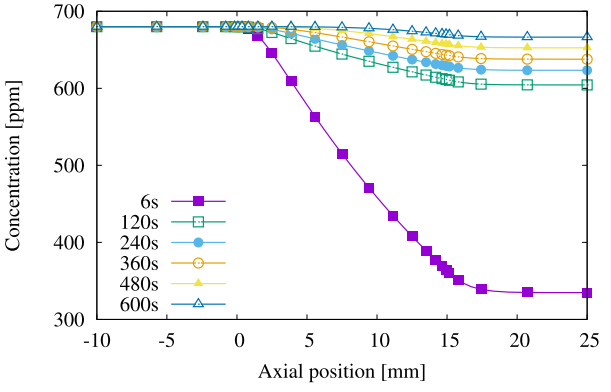

Figure 9. NO_2 concentration along the axis of the channel at different time during the first 600 s of test with a time interval of about 2 minutes. A constant concentration of 680 ppm of NO_2 is imposed at the inlet.

3.1. Description of the NO_2 inlet phase

The concentration of NO_2 along the axis of the channel, during the flowing of NO_2 in the first 600 s of test, is reported in Figure 9. At t = 6 s, the adsorption of NO_2 on the BaO sites is maximum, reaching an NO_2 reduction of about 51%. The minimum NO_2 concentration at the centerline is reached after the end of the active channel, x = 15 mm, due to the inertial effect of the flow. After 2 minutes, t = 120 s, the NO_2 reduction diminishes at about 11% and continues to decrease according to the saturation of BaO sites with NO_2. On the other hand, the NO concentration at the exit increases monotonically from the inlet to the outlet (Figure 10). According to the continuous saturation of the active site of BaO on the washcoat, the increase of NO along the channel diminishes with respect to the time. Therefore, at the end of the NO_2 phase, at t = 600 s, the outlet concentration of NO reaches its minimum. In Figure 11 the contours of the NO_2 concentrations on the longitudinal plane section along the axial direction is reported at the end of the NO_2 inlet phase,

 https://doi.org/10.1016/j.heliyon.2018.e00529

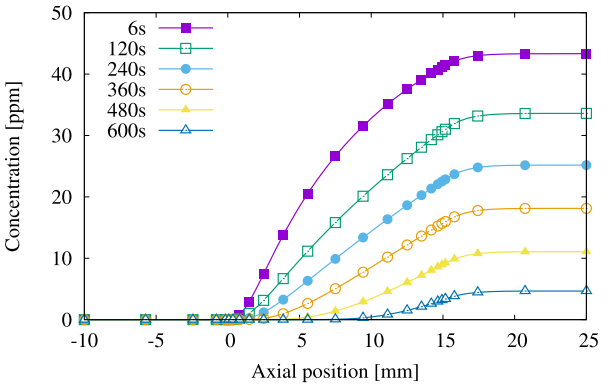

Figure 10. NO concentration along the axis of the channel at different time.

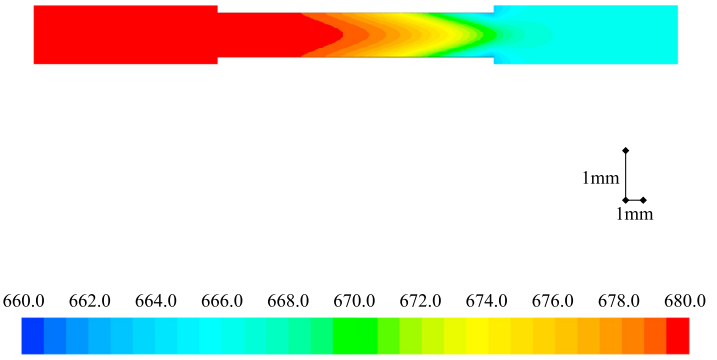

Figure 11. Contours of the NO2 concentrations, ppm, along the meridian plane at $t = 600$ s.

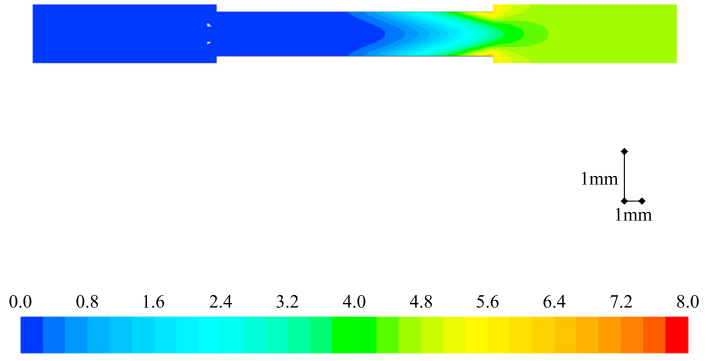

Figure 12. Contours of the NO concentrations, ppm, along the meridian plane at $t = 600$ s.

at $t = 600$ s. At this stage, as already reported in the previous description, the BaO is almost saturated, therefore the catalyst determines just a small reduction of the inlet concentration of NO_2, from 680 ppm to about 665 ppm in the final part of the channel. Similarly, the NO release from the catalyst takes place mainly near the channel exit, according to the BaO saturation of the upstream region of the channel (Figure 12). Differently from circular ducts, the square section of the channel induces a well-known complex flow field distribution due to secondary

 https://doi.org/10.1016/j.heliyon.2018.e00529

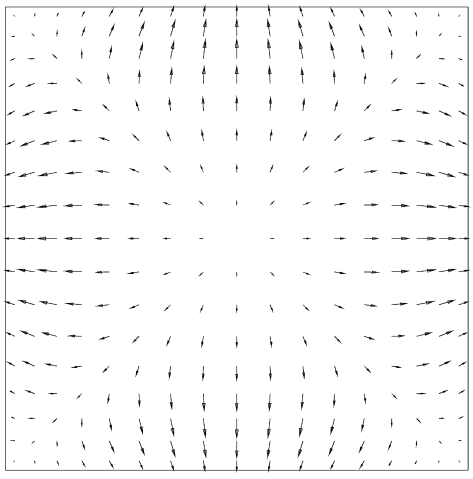

Figure 13. Instantaneous velocity vectors, in m/s, at the channel outlet transversal section, $x = 15$ mm, at $t = 600$ s.

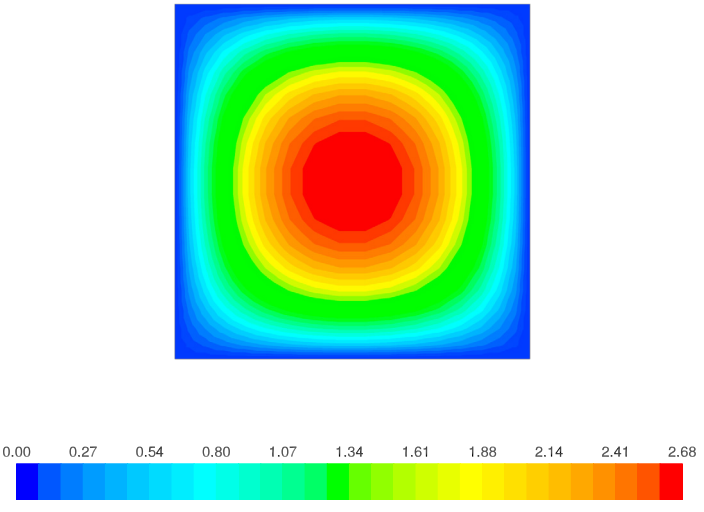

Figure 14. Instantaneous contours of the axial velocity, m/s, at the channel outlet transversal section, $x = 15$ mm, at $t = 600$ s.

flows, as reported in Figure 13, which can be recognized in a transversal section of the channel by means of transversal components of the velocity vectors. Two symmetry planes are aligned along to the diagonals of the square. The secondary flows are characterized by a radial behavior from the center toward the square sides. In Figure 14, the axial velocity remarks the laminar characteristic of the flow, due to the small Reynolds number. However, because of the square section, the axial velocity reduction is enhanced near the square corners. Thus, the spatial distribution of the flow is expected to influence the conversion efficiency of the catalytic surface of the channel. The contours of NO_2 over the outlet section of the channel (see Figure 15) highlights the minima of the concentrations near the corners. The minima can be found just close to the corner position, as reported in the concentration curve

 https://doi.org/10.1016/j.heliyon.2018.e00529

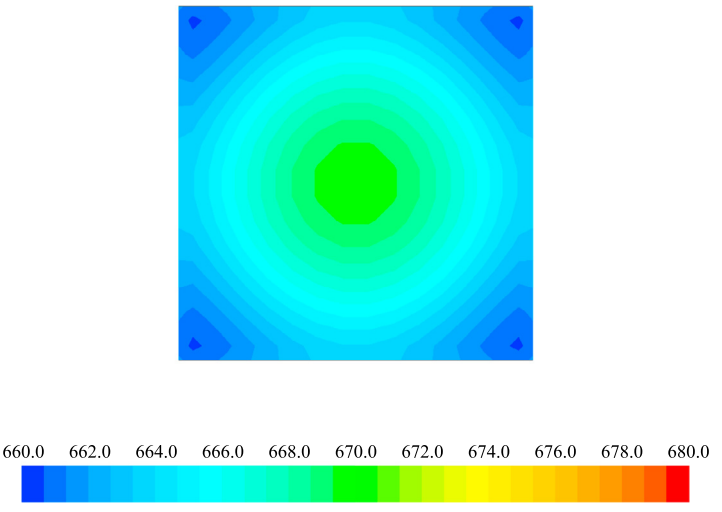

Figure 15. Contours of the NO2 concentrations, ppm, on a transversal slice at the channel outlet (x = 15 mm) at t = 600 s.

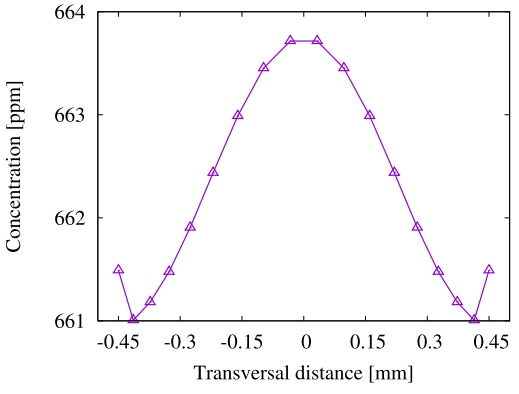

Figure 16. Surface NO_2 concentrations, ppm, on the side of the channel outlet (x = 15 mm) with respect to the transversal distance from the centerline. The data are spatially averaged with respect the 4 side of the square channel. The curve correspond to t = 600 s.

of NO_2 along the side of the square section, see Figure 16. On the other hand, looking at Figures 17, 18 the NO concentrations have an opposite behavior with respect to the NO_2 concentration with a maximum at the center of the wall sides and two symmetrical maxima just close to the corners.

3.2. Description of the NO inlet phase with temperature ramp

After 60 s of inert flowing of N_2, a NO flux of 600 ppm is considered. The temperature has been kept constant at 350 °C till t = 900 s, giving a steady condition in which the catalyst is not able to sensibly change the inlet concentration of NO, as shown in Figure 6. The results remark the good approximation of the model with respect to the experimental data. In Figure 19 the O_2 concentration along the

 https://doi.org/10.1016/j.heliyon.2018.e00529

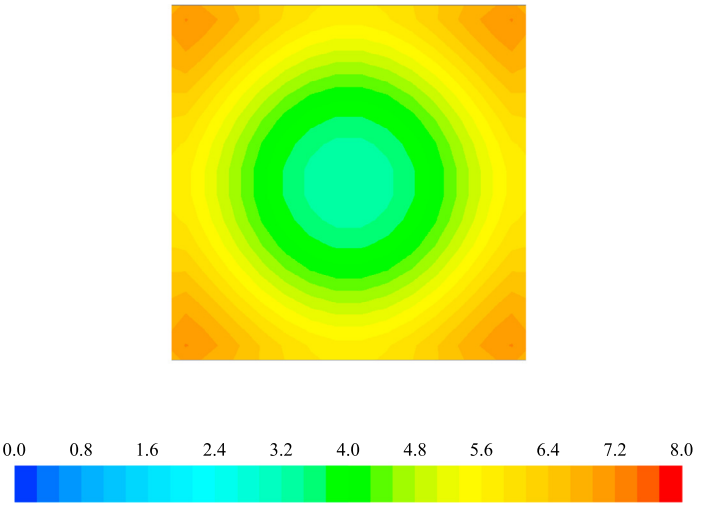

Figure 17. Contours of the NO concentrations, ppm, on a transversal slice at the channel outlet (x = 15 mm) at t = 600 s.

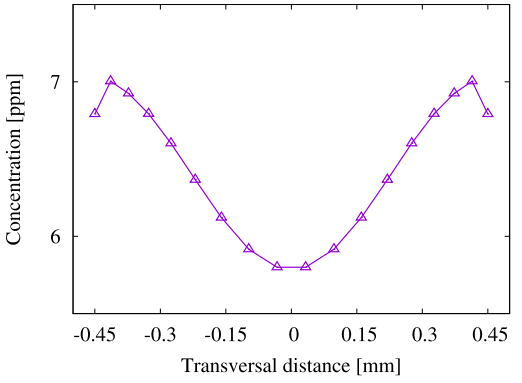

Figure 18. Surface NO concentrations on the side of the channel outlet (x = 15 mm) with respect to the transversal distance from the centerline. The data are spatially averaged with respect the 4 side of the square channel. The curve correspond to t = 600 s.

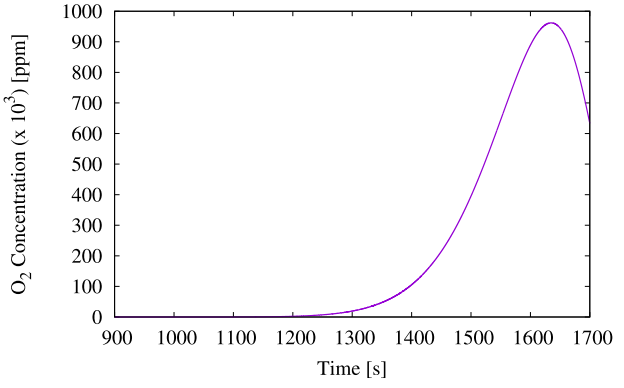

Figure 19. Surface averaged O_2 concentration at the channel outlet with respect to the time during the NO phase with temperature increasing, (t = 900 s–1700 s).

 https://doi.org/10.1016/j.heliyon.2018.e00529

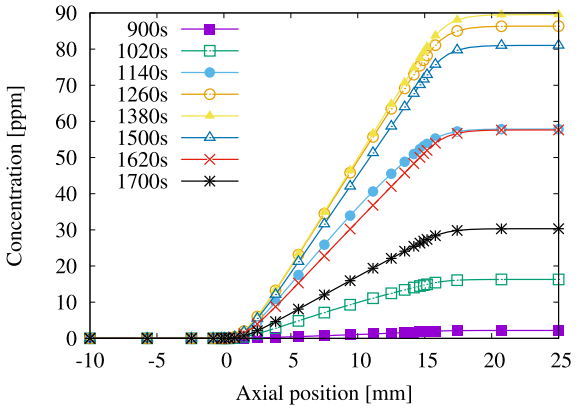

Figure 20. NO_2 concentration along the axis of the channel at different for $t = 900$ s–1700 s of test with a time interval of 2 minutes.

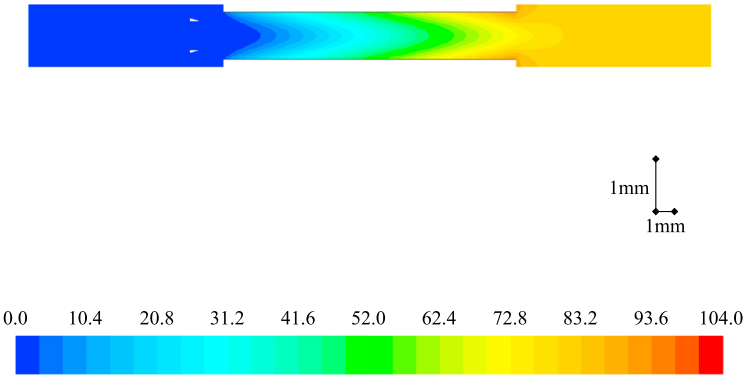

Figure 21. Contours of the NO2 concentrations, ppm, along the meridian plane at $t = 1500$ s.

temperature ramp ($20\,°C/min$) reveals that the O_2 release starts at $t > 1200$ s, according to the temperature increase as remarked also in the work of Nova et al. (2004). In Figure 20, the NO_2 concentration along the channel axis has an increasing behavior. The maximum NO_2 concentration corresponds at $t = 1380$ s, whereas the O_2 concentration with respect to the time shows a maximum at about 1600 s. Therefore, a considerable delay between NO_2 and O_2 appears. This behavior can be related to the saturation of BaO–O and the temperature increase, that induce the production of O_2 due to the balance of reaction $R5$ (see Table 2). Moreover, reactions $R2$ and $R3$ are directly related to this effect. Thus, the $R2_f$ and $R3_b$ increase their kinetic rate with respect to the temperature, being the $R2_b$ and $R3_f$ not activated ($E = 0$) (see Table 3). Indeed these reactions involve the surface species BaO–O and volumetric species, NO_2 and NO. According to the fluid dynamics effects, described in the previous section, non homogeneous spatial distribution of the species is expected. In Figure 21, NO_2 distribution along the longitudinal symmetry plane of the domain has been reported at $t = 1500$. The activation of the catalytic mechanism produces NO_2 along the channel, therefore there is a spatial increasing of NO_2

 https://doi.org/10.1016/j.heliyon.2018.e00529

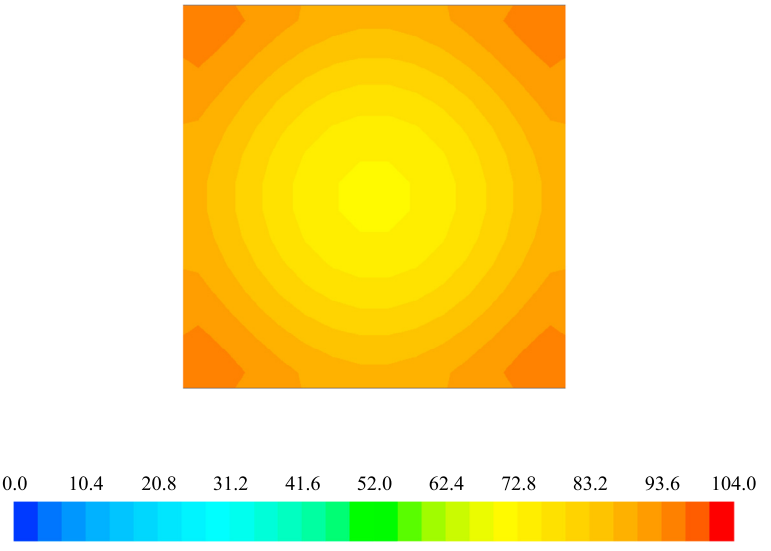

Figure 22. Contours of the NO2 concentrations, ppm, on a transversal slice at the channel outlet (x = 15 mm) at t = 1500 s.

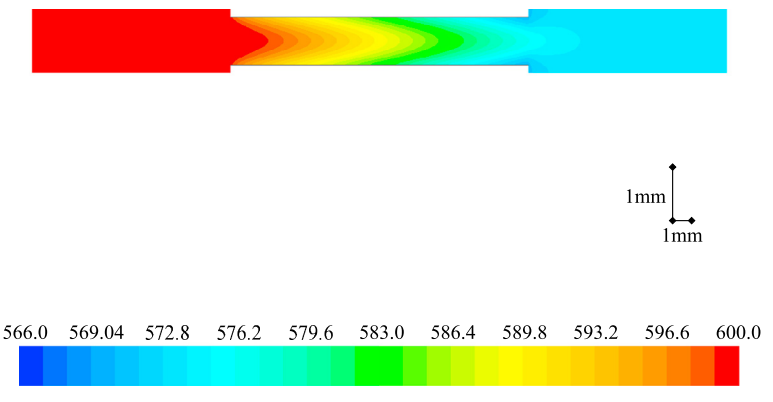

Figure 23. Contours of the NO concentrations, ppm, along the meridian plane at t = 1500 s.

concentration that ranges from 0 ppm at the inlet, to about 90 ppm at the outlet. More details of the spatial distribution of the NO_2 concentration are reported in Figure 22, where a transversal slice at the active channel outlet (x = 15 mm) is reported. Thus, near the corners a higher concentration with respect to the axial value appears, confirming the influence of the corners on the catalyst behavior. Accordingly, the NO spatial behavior at the same instant is reported in the same slice position used for the description of NO_2 species. In Figure 23, the NO abatement along the channel axis is evident. At t = 1500 s the NO concentration decreases from 600 ppm, imposed at the inlet, to about 570 ppm. The outlet transversal section confirms the catalyst behavior previously described (see Figure 24). Indeed, the lower NO concentration with respect to the axial value is consistent to the distance from the active catalytic surface.

 https://doi.org/10.1016/j.heliyon.2018.e00529

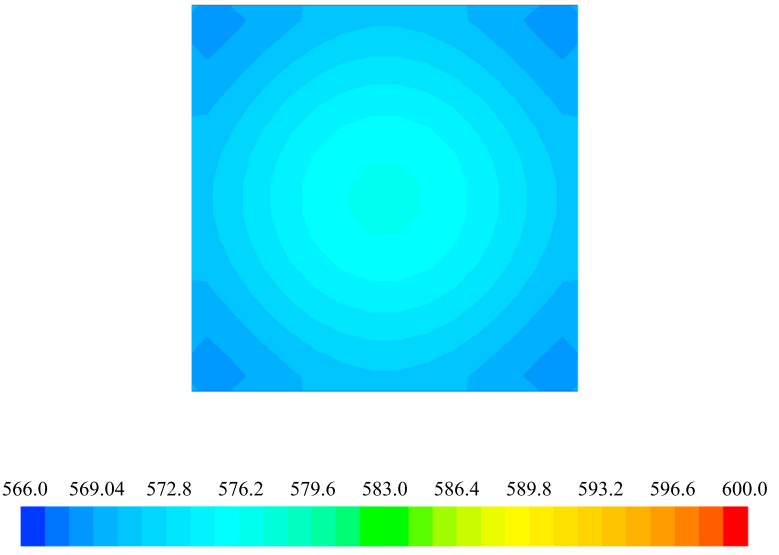

Figure 24. Contours of the NO concentrations, ppm, on a transversal slice at the channel outlet ($x = 15$ mm) at $t = 1500$ s.

4. Conclusions

A single square catalyst channel has been studied by means of a numerical model in order to take into account both the fluid dynamic effects and the superficial chemical reactions. The existent chemical model gives a good prediction of the overall input/output catalyst performance in terms of chemical behavior. On the other hand, the fluid dynamics of the laminar flow within a square channel influences the spatial distribution of the different species within the catalyst. In this paper we shed light to the influence of flow-chemical interaction on the catalyst performance. The test has been based on data available in the literature on a catalyst having as active sites only BaO. The comparison against data confirms the reliability of the method. The details of the temporal and spatial behavior of all the species involved in the mechanism are reported. The three-dimensional distributions of the species reveal the axial gradient of the chemical mixture composition, as expected. Moreover, transversal spatial distributions over the square section result to be non homogeneous, according to the secondary flows and boundary effects of the walls. Hence, the corners of the square section appear to influence both the spatial distribution of the flow and the species concentrations. Even though simplified model can predict with a small effort the same overall input/output performance of a catalyst, the present investigation highlights non uniformity in the conversion efficiency of a single catalytic square channel of a multi-channels monolith. The coupling of numerical fluid dynamics with chemical models appears a promising tool for the detailed study and optimization of catalysts.

 https://doi.org/10.1016/j.heliyon.2018.e00529

Declarations

Author contribution statement

Francesco Fornarelli: Conceived and designed the experiments; Performed the experiments; Analyzed and interpreted the data; Contributed reagents, materials, analysis tools or data; Wrote the paper.

Ruggiero Dadduzio: Performed the experiments; Analyzed and interpreted the data; Contributed reagents, materials, analysis tools or data.

Sergio Mario Camporeale, Marco Torresi and Bernardo Fortunato: Conceived and designed the experiments; Performed the experiments; Analyzed and interpreted the data.

Funding statement

This work was supported by the European Union (EU), Italian Ministry of Economic Development (MISE), Italian Ministry of University and Research (MIUR) and Apulia Region through project “NanoApulia”, project n. MDI6SR1.

Competing interest statement

The authors declare no conflict of interest.

Additional information

No additional information is available for this paper.

References

Benjamin, S., Roberts, C., 2007. Three-dimensional modelling of NO_x and particulate traps using CFD: a porous medium approach. Appl. Math. Model. 31, 2446–2460.

Bhatia, D., McCabe, R.W., Harold, M.P., Balakotaiah, V., 2009. Experimental and kinetic study of NO oxidation on model Pt catalyst. J. Catal. 266, 106–119.

Cao, L., Ratts, J.L., Yezerets, A., Currier, N.W., Caruthers, J.M., Ribeiro, F.H., Delgass, W.N., 2008. Kinetic modeling of NO_x storage/reduction on $Pt/BaO/Al_2O_3$ monolith catalyst. Ind. Eng. Chem. Res. 47, 9006–9017.

 https://doi.org/10.1016/j.heliyon.2018.e00529

Chen, M., Aleixo, J., Williams, S., Leprince, T., 2004. CFD modelling of 3-way catalytic converters with detailed catalytic surface reaction mechanism. SAE Int. 0148.

Corbetta, M., Manenti, F., Visconti, C.G., 2014. CATalytic – Post Processor (CAT-PP): a new methodology for the CFD-based simulation of highly reactive heterogeneous system. Comput. Chem. Eng. 60, 76–85.

Fornarelli, F., Camporeale, S., Dadduzio, R., Fortunato, B., Torresi, M., 2015. Numerical simulation of the flow field and chemical reactions within a NSC diesel catalyst. Energy Proc. 82, 381–388.

Kočí, P., Štěpánek, F., Kubíček, M., Marek, M., 2006. Meso-scale modelling of CO oxidation in digitally reconstructed porous Pt/γ-Al_2O_3 catalyst. Chem. Eng. Sci. 61, 3240–3249.

Koop, J., Deutschmann, O., 2007. Modeling and simulation of NO_x abatement with storage/reduction catalyst for lean burn and diesel engines. SAE Technical Paper 2007-01-1142. https://doi.org/10.4271/2007-01-1142.

Koop, J., Deutschmann, O., 2009. Detailed surface reaction mechanism for Pt-catalyzed abatement of automotive exhaust gases. Appl. Catal. B, Environ. 91, 47–58.

Kota, A.S., Luss, D., Balakotaiah, V., 2015. Micro-kinetic of NO_x storage and reduction with H_2/CO/C_3H_6 on Pt/BaO/Al_2O_3 monolith catalyst. Chem. Eng. J. 262, 541–551.

Larson, R.S., Chakravarthy, V.K., Pihl, J.A., Daw, C.S., 2012. Microkinetic modeling of lean NO_x trap chemistry. Chem. Eng. J. 189–190, 134–147.

Laurent, F., Pope, C., Mahzoul, H., Delfosse, L., Gilot, P., 2003. Modelling of NO_x adsorption over NO_x adsorbers. Chem. Eng. Sci. 58, 1793–1803.

Lindholm, A., Currier, N.W., Li, J., Yezerets, A., Olsson, L., 2008. Detailed kinetic modeling of NO_x storage and reduction with hydrogen as the reducing agent and in the presence of CO_2 and H_2O over Pt/Ba/Al catalyst. J. Catal. 258, 273–288.

Maestri, M., Cuoci, A., 2013. Coupling CFD with detailed microkinetic modeling in heterogeneous catalysis. Chem. Eng. Sci. 96, 106–117.

Mihet, M., Cristea, V.M., Agachi, P.S., Cormos, A.M., Lazar, M.D., 2016. CFD simulations, experimental validation and parametric studies for the catalytic reduction of no by hydrogen in a fixed bed reactor. R. Soc. Chem. Adv. 6, 89259–89273.

Nova, I., Castoldi, L., Lietti, L., Tronconi, E., Forzatti, P., Prinetto, F., Ghiotti, G., 2004. NO_x adsorption study over Pt–Ba/alumina catalysts: FT-IR and pulse experiments. J. Catal. 222, 377–388.

Olsson, L., Blint, R.J., Fridell, E., 2005. Global kinetic model for lean NO_x trap. Ind. Eng. Chem. Res. 44, 3021–3032.

Olsson, L., Persson, H., Fridell, E., Skoglundh, M., Andersson, B., 2001. A kinetic study of NO oxidation and NO_x storage on Pt/Al_2O_3 and $Pt/BaO/Al_2O_3$. J. Phys. Chem. B 105, 6895–6906.

Rankovic, N., Nicolle, A., Costa, P.D., 2010. Detailed kinetic modeling study of NO_x oxidation and storage and their interactions over $Pt/Ba/Al_2O_3$ monolith catalyst. J. Phys. Chem. C 114, 7102–7111.

Roy, S., Baiker, A., 2009. NO_x storage-reduction catalysis: from mechanism and materials properties to storage-reduction performance. Chem. Rev. 109, 4054–4091.

Scotti, A., Nova, I., Tronconi, E., Castoldi, L., Lietti, L., Forzatti, P., 2004. Kinetic study of lean NO_x storage over $Pt–Ba/Al_2O_3$ system. Ind. Eng. Chem. Res. 43, 4522–4534.

Shwan, S., Partridge, W., Choi, J.S., Olsson, L., 2014. Kinetic modeling of NO_x storage and reduction using spatially resolved MS measurements. Appl. Catal. B, Environ. 147, 1028–1041.

Štěpánek, J., Kočí, P., Marek, M., Kubíček, M., 2012. Catalyst simulation based on coupling of 3D CFD tool with effective 1D channel models. Catal. Today 188, 87–93.

Wickman, B., Lundström, A., Sjöblom, J., Creaser, D., 2007. Modeling mass transport with microkinetics in monolithic NO_x storage and reduction catalyst. Top. Catal. 42–43, 123–127.

Xu, J., Clayton, R., Balakotaiah, V., Harold, M.P., 2008. Experimental and microkinetic modeling of steady-state NO reduction by H_2 on $Pt/BaO/Al_2O_3$ monolith catalyst. Appl. Catal. B, Environ. 77, 395–408.

Xu, J., Harold, M.P., Balakotaiah, V., 2009. Microkinetic modeling of steady-state $NO/H_2/O_2$ on $Pt/BaO/Al_2O_3$ NO_x storage and reduction monolith catalyst. Appl. Catal. B, Environ. 89, 73–86.